Ceramics International 43 (2017) 11759–11765

Contents lists available at ScienceDirect

Ceramics International

journal homepage: www.elsevier.com/locate/ceramint

Mechanical behavior and microstructure of porous needle: Aluminum borate ($Al_{18}B_4O_{33}$) and Al_2O_3-$Al_{18}B_4O_{33}$ composites

María F. Hernández[a,b,*], Gustavo Suárez[a,b], Mariano Cipollone[b,c], Esteban F. Aglietti[a,b], Nicolás M. Rendtorff[a,b]

[a] Centro de Tecnología de Recursos Minerales y Cerámica CETMIC (CIC-CONICET), Cno. Centenario y 506 Gonnet, La Plata (1897), Argentina
[b] Departamento de Química, Facultad de Ciencias Exactas UNLP, 47 y 115, La Plata (1900), Argentina
[c] Química Analítica, Y-TEC SA, Av. Del Petróleo s/n 1923, Berisso, Buenos Aires, Argentina

ARTICLE INFO

Keywords:
Porous ceramics
Aluminum borate
Properties
Mechanical behavior
Diametral compression

ABSTRACT

In this article we assess and compare the complex mechanical behavior of two complex microstructure ceramics material formed within the reaction sintering framework

Two comparable pairs of materials with respectively similar microstructures were obtained by reaction sintering from boric acid and alumina. Two single phase porous ceramics were compared with two composite (1:1) porous ceramic. The first and second phases were aluminum borate needles ($Al_{18}B_4O_{33}$) and alumina (Al_2O_3).

The four with comparable grain size and analogous apparent porosities: in diameter (≈ 0.7 μm) and in volume fraction (≈ 45%). The mechanical behavior was studied by means of the diametral compression test at low displacement rate and explained in terms of the texture, microstructure features evaluated by mercury intrusion porosimetry and scanning electron microscopy.

Single $Al_{18}B_4O_{33}$ phase porous materials presented higher mechanical strengths than the composite materials. Within the respective microstructural configurations the whisker thickness did not affect significantly the mechanical behavior and parameters. A well-defined fragile behavior was observed and described in the composite material. On the other hand the single $Al_{18}B_4O_{33}$ needle porous material presented a distinctive behavior with local discontinuities without loss of integrity in the diametral stress behavior, and achieved strength up to 50% higher than the corresponding composite.

1. Introduction

Composite materials have an important industrial and technological role in technological ceramics. The designing capability of the manufacturer in properties and behaviors is enhanced by combining two or more different materials. However, the final properties will not always be between the pure material ones; in fact, in several cases the properties are considerably improved. The final properties and behaviors will always be related to the actual microstructural configuration. The actual relation has to be established for better microstructural design.

Porous ceramics present a wide range of characteristics that result in a wide collection of technological applications, like filtration, absorption, catalysts and catalyst supports, lightweight structural components and thermal insulators. Particularly in the present article we make focus on the microstructure-mechanical behavior relation.

Different processing routes have been proposed, explored and established. These include partial sintering, sacrificial fugitives, replica templates and direct foaming [1]. Depending on requirements, it is also possible to combine various methods to further fine-tune the characteristics of the porous ceramics [2,3]. The general properties of porous ceramics were completely reviewed in a recent article by Ohji and Fukushima in 2012.

The partial sintering, the most conventional technique for making porous ceramics, has been substantially sophisticated in recent years. Very homogeneous porous ceramics with extremely narrow size distribution have been successfully prepared through sintering combined with in situ chemical synthesis. Carefully tailored micro-structure (size, morphology and even orientation of grains and pores, etc.) of porous ceramics has led to unique mechanical properties, which cannot be attained even in the dense materials [2,3].

Alumina and alumina based composite materials are a family of ceramics whose principal constituent is aluminum oxide (Al_2O_3). On a

* Corresponding author at: Centro de Tecnología de Recursos Minerales y Cerámica CETMIC (CIC-CONICET) Cno., Centenario y 506 Gonnet, La Plata (1897), Argentina.
E-mail address: florenciahernandez@cetmic.unlp.edu.ar (M.F. Hernández).

http://dx.doi.org/10.1016/j.ceramint.2017.06.011
Received 23 May 2017; Received in revised form 31 May 2017; Accepted 3 June 2017
Available online 03 June 2017

Table 1
Physical properties of the studied phases.

	Thermal Conductivity λ_i (W/m K)	Density (g/cm^3)	Young modulus (GPa)	Strength (MPa)	Hardness (Mohs)	Thermal expansion $\times 10^{-6}$ °C^{-1}
Alumina (Al_2O_3)	18–25	3,95	300	300	9	≈ 8
Aluminum borate ($Al_{18}B_4O_{33}$)	4–6	2,96	400	8000	7	≈ 4.5 (axial) ≈1.9 (radial)

weight basis, these materials have the largest share of the ceramics' world market [4] with multiple applications. Alumina presents high refractoriness, that is, high melting point (2050 °C) and retention of structural integrity at a high temperature. In particular, it experiences practically no deformation under compressive loads at temperatures up to 1200 °C [4].

Boron-aluminate materials (between $Al_{18}B_4O_{33}$ and $Al_4B_2O_9$) present a high refractoriness accompanied by chemical inertness in some environments [5], the presence of catalytic properties for some technological reactions is also remarkable [6–8]. These phases present a strong needle morphology tendency [9–11]. Table 1 compares the physical properties of alumina and aluminum borate [11,12].

The utilization of aluminum borates needles or whiskers for aluminum and aluminum based alloys reinforcement are the principal application of these phases [11]. Reinforcing magnesium alloys was proposed as well [13]. The mechanical behavior of the material, the chemical compatibility (low wettability) of the borate phase with metallic aluminum and the microstructural configuration of the metal-ceramic composites encourages these particular applications. The mechanical behavior of the composites is higher than the behavior of the corresponding metallic materials.

As mentioned, refractory and other structural applications were reported, these materials were proposed as insulating and filtering materials as well. Besides the reaction sintering from alumina and Boric oxide [14–16] some synthetic routes have been proposed and studied, these include: the flux method [17], crystallization from molten salts [18], sol-gel routes and chemical precursors [19–22], combustion synthesis route was studied as well [8]. Besides, alumina or metallic aluminum was proposed as the aluminum source [23,24]. Vitro-ceramics with aluminum borates as crystalline phase were also studied and presented technological properties [25]. Electrospinning routes are also being studied [26].

Several studies had been recently carried out respect to the incorporation of boron oxide containing compounds in refractory materials, like alumina, magnesia and mullite based castables [27–32]. The boron oxide containing compounds were proposed as effective ceramic mineralizers during thermal treatments of the refractory castables achieving the in situ formation of new crystalline phase with mechanical behavior enhancements. This shows the actual potentiality of the boron containing materials in the refractory industry.

In a recent article a series of porous (≈45%) refractory materials from the Al_2O_3-B_2O_3 system were developed. The processing strategy resulted in materials with BA: $Al_{18}B_4O_{33}$ as the main phase accompanied by alumina or unique crystalline phase. Needle grains with diameters between 0.2 and 1 μm and an aspect ratio over 20:1 were obtained [33]. The developed monoliths obtained by direct reaction sintering of boric acid and calcined alumina presented almost 50% of porosity.

The mechanical resistance, stiffness and the overall mechanical behavior of materials ought to be described if the application of a selected material is proposed. This is the case of aluminate needle borate based monolithic porous materials, especially for structural applications.

In this article we intend to assess and compare the complex mechanical behavior of two complex microstructure ceramics material formed within the reaction sintering framework; and to understand this behavior with the microstructural features of the studied set of materials. And will provide information for further microstructure design strategies and technological applications.

Particularly two pairs of materials with respectively comparable microstructures were processed by reaction sintering from boric acid and alumina; two single phase porous materials with aluminum borate as unique crystalline phase (AB: $Al_{18}B_4O_{33}$) were compared with two alumina – aluminum borate composite ceramics.

The four materials present comparable grain size and comparable apparent porosities: in diameter (≈ 0.7 μm) and in volume fraction (≈ 45%).

2. Experimental procedures

2.1. The materials

A set of four porous ceramic materials were studied, labels and their properties are shown in Table 2. Calcined alumina (alumina A2G, ALCOA) and boric acid (Borax Argentina SA) were employed as starting powders. Intimate mixtures were obtained by ethanol mixture. Dried powder was then pressed in disc shape samples that were fired with a 5 °C/min heating rate, in air atmosphere, up to 1200 and 1300 °C with 120 min soaking. A wider description of the starting powders, processing conditions, the actual thermal formation and

Table 2
Principal characteristics of the studied materials.

Sample label	Microstructural configuration	Firing temperature (°C)	Initial B_2O_3 (wt%)	Volumetric Density (g/cm^3)	Open Porosity (%)	Crystalline phases content In weight basis (wt%)			Effective thermal conductivity[a]
						Al_2O_3	$Al_{18}B_4O_{33}$	$Al_4B_2O_9$	λ (W/m K)
C_{PM}1200	Porous Composite	1200	13.0	1.93	43.5	55.8	43.1	1.1	6.4
C_{Pm}1300		1300		1.91	39.3	58	42.0	Traces	6.9
SP_{PM}1200	Porous	1200	26.0	1.78	47.0	5	93.3	1.7	2.9
SP_{PM}1300	single phase	1300		1.75	45.4	0.7	97.4	1.9	2.7

[a] Calculated using Eq. (1).

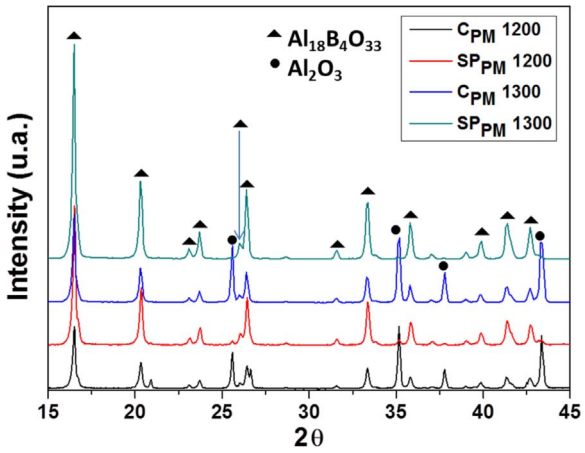

Fig. 1. XRD patterns of the studied materials.

other properties can be found elsewhere [33]. While the first material, C_{PM}, can be described as an alumina –aluminum borate porous composite, the second one (SP_{PM}) can be described as a single phase aluminum borate porous body. The achieved porosity is within 40–45%. The apparent density is around 1.9 g/cm^3 for composite materials C_{PM1200} and C_{PM1300} and around 1.8 g/cm^3 for the SP_{PM} materials.

Fig. 1 presents the powder X-ray diffraction patterns of the studied materials, this confirms the aluminum borate ($Al_{18}B_4O_{33}$) presence as the principal crystalline phase for SP_{PM}, and this was only accompanied by corundum (Al_2O_3) diffractions, marked in C_{PM}. The evaluated phase content is shown in Table 2; no amorphous phase can be observed. The quantification was performed by the Rietveld method [33]. The slight stoichiometric discrepancies might be explained by the non-stoichiometric nature of the borates [23,24] and the accuracy of the Rietveld refinements employed for evaluating the crystalline phases content. Table 2 also presents the principal properties of the studied materials together with the initial boric acid employed in the synthesis and the used labels. The thermal conductivity (λ) of the developed porous materials was estimated by a simple mixing rule calculation, employing the volumetric fractions (V_i) evaluated by the Rietveld method. Employing the following equation:

$$\lambda = \sum_{i}^{n} \lambda_i . V_i \quad (1)$$

Where λ_i corresponds to the thermal conductivity of each crystalline phase.

The calculated thermal conductivities of the materials (Table 2) are similar within the microstructural configuration. It is worth to point out that the single phase porous materials presents a lower thermal conductivity due to the lower thermal conductivity of the borate in comparison to the corundum (Table 1).

2.2. Characterizations and techniques

Porosity is relevant in ceramic microstructural properties and involves mechanical resistance (strength, hardness, stiffness); electrical and thermal conductivity; chemical erosion; permeability; adsorption; and refractoriness properties. For this, mercury intrusion tests were performed by using a Porosimeter 2000 Carlo Erba and pressures ranging from 1 to 2000 kg/cm^2 [34]. The developed microstructures were evaluated by scanning electron microscopy (SEM-JEOL JMS-6000, Japan). A particle size analysis was carried out.

The diametral compression test, also known as “splitting test” or “Brazilian test”, has usually been employed in the mechanical evaluation due to several advantages: simpler piece preparation, simple geometry and quickness of testing, independent data with regard to surface finish and no edge effects [35–38]. In this case, the 15 mm diameter and 5 mm thick disc-shaped samples were diametrically compressed in a universal mechanical testing machine (INSTRON 5985, USA), at a constant strain rate of 0.1 mm/min, with steel plates. Lubricant paste was applied on the platen surfaces in contact with the disc to reduce the effect of friction; white and carbon papers were placed together between each platen and the disc for load distribution (padding material). The initial diameter was used for the calculation, and L was employed for the final maximum load of samples. For this method, the mechanical strength and displacement can be calculated with the following equations:

$$\sigma_d = \frac{2L}{\pi DT} \quad (2)$$

$$\varepsilon = \frac{\Delta d}{D} \quad (3)$$

Where L is the final load, D is the initial diameter, T is the thickness of the disc-shaped sample and Δd is the universal testing machine displacement.

At least 8 samples were evaluated for each material. The differences between probes dimensions were below 2%. This assumption is implicit in the theoretical treatment of the diametral compression loading case [35,37,39,40]. From the experimental load versus displacement curve, the stress (σ_d) versus strain (ε) curves were obtained. The following parameters were determined: mechanical strength (σ_d) using the maximum peak load and the apparent Young modulus (E_d) as the slope of the final portion of the stress-strain curve before the sudden collapse. The final 25% of the curve before the sudden breakage was employed for calculating this parameter.

3. Results and discussions

3.1. Porosimetry (DP_{50})

The evaluated pore size distributions can be observed in Fig. 2. Table 3 shows the pore size percentiles. The mean pore size is the same for the four studied materials (≈ 700 nm). This fact sustains the whole behavior comparison hypothesis carried out in this study. The achieved distribution width is higher for the single phase (SP_{PM}) materials. $SP_{PM}1200$ distribution is slightly narrower than $SP_{PM}1300$, almost below the micron. It is worth to point out that the porosity size is in all the cases over the 100 nm. This brings important information for possible microfiltration applications.

On the other hand the appearance of some macropores (2–5 μm) fraction can be observed in the SP_{PM}: 20% for the $SP_{PM}1200$ 10% for

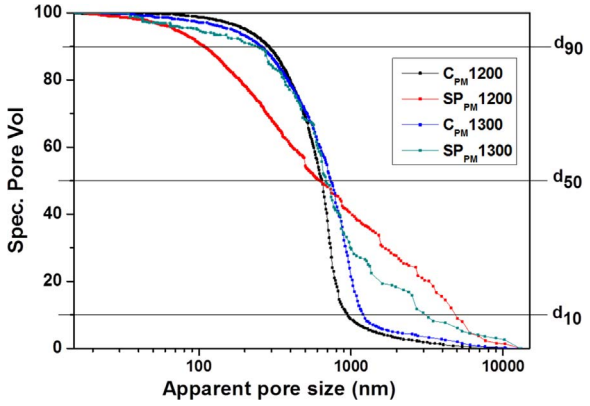

Fig. 2. Open pore size distribution of the studied materials by Mercury Intrusion Porosimetry.

Table 3
Pore size diameters of the studied materials.

Sample	d_{10} (nm)	d_{50} (nm)	d_{90} (nm)
C_{PM} 1200	960	643	300
C_{PM} 1300	1230	736	250
SP_{PM} 1200	4960	643	110
SP_{PM} 1300	3120	694	250

SP_{PM}1300. From this it can be inferred that the further thermal coalescence (thickening) of the AB needles results in a decrease in the macroporosity. There are no important differences between C_{PM}1200 and C_{PM}1300.

3.2. Microstructural characterization of the studied materials by SEM

The open porosities are comparable: ≈ 40% for the C_{PM} and ≈ 45% for the SP_{PM} materials. Fig. 3 shows the SEM images of materials C_{PM}1200, C_{PM}1300, SP_{PM}1200 and SP_{PM}1300 at two different magnifications. Free fracture, gold coated, observations were performed. The whisker or nano-rod morphology can be identified in the four materials. The effect of the initial alumina: boron ratio is evident; some important amount of unreacted rounded alumina particles are imbibed in a whisker matrix for the C_{PM} materials. In fact, there's a half of alumina in terms of volume fraction. After the Rietveld phase quantification, together with the open porosity figures, the volume fraction composition of the studied materials was estimated, this is compared in Fig. 3 as well. These were estimated assuming theoretical

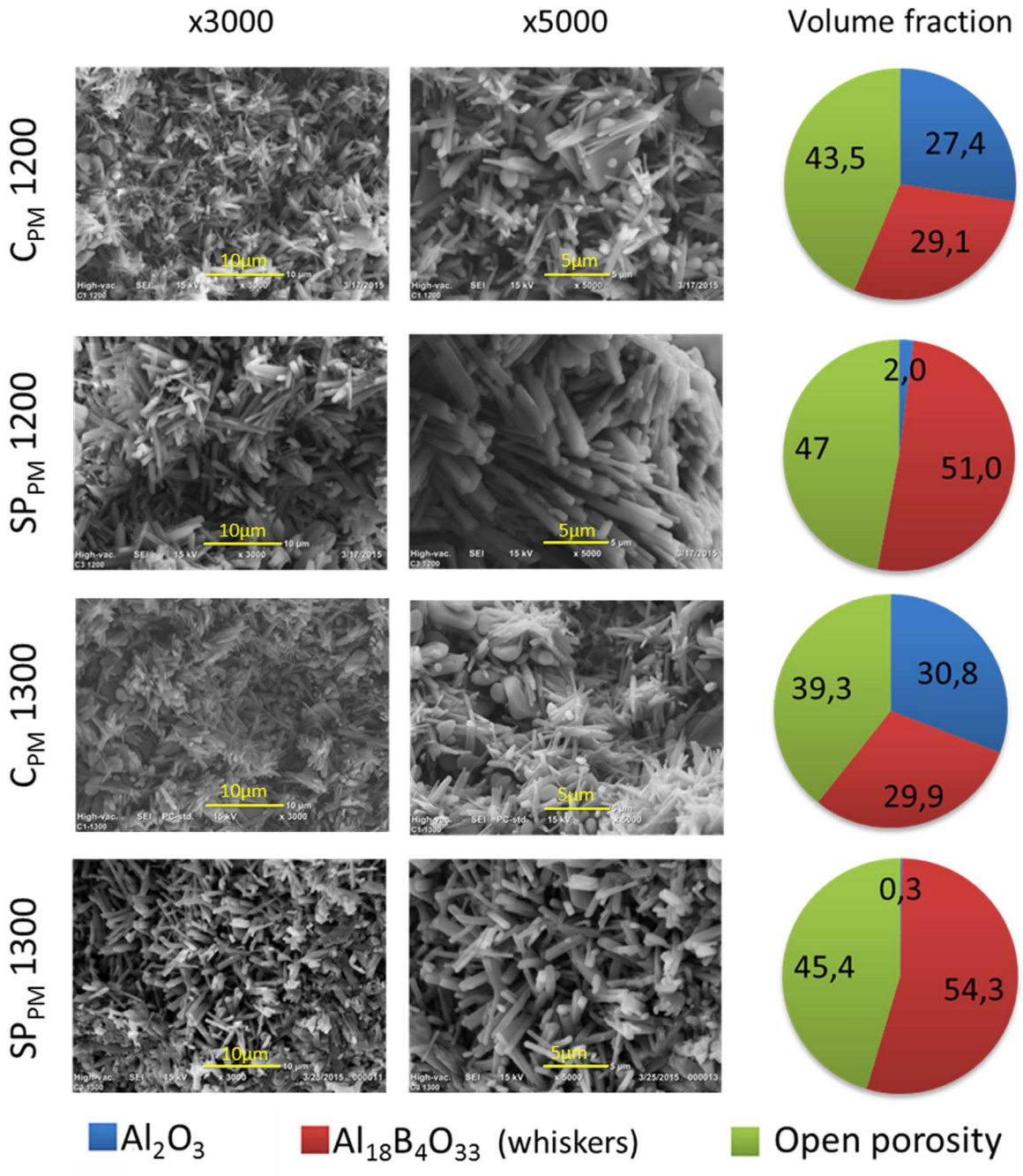

Fig. 3. SEM images (×3000 and ×5000) and volume fraction composition of the SP_{PM} and C_{PM} materials.

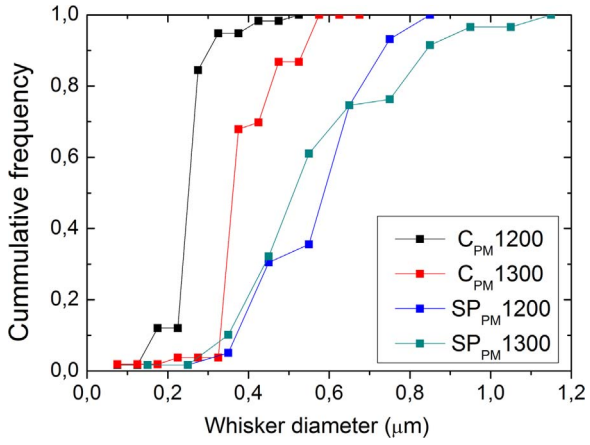

Fig. 4. Whisker diameter distribution of the studied materials.

densities of 3.95 g/cm^3 and 2.95 g/cm^3 for the alumina and the aluminum borate respectively. The observed results are in concordance with the observed microstructure.

In Fig. 4, whisker thickness was assessed from the SEM images, shown in Fig. 3. Neither alumina grains' nor needles' length were possible to evaluate accurately. SP_{PM} needle diameters (around 0.6 μm) are equivalent for the two performed thermal cycles. C_{PM} needle diameter is around half of the SP_{PM} materials needle diameter. The whisker thickness after this particular thermal treatment was enhanced by the thermal cycle maximum temperature in C_{PM}.

The alumina grain size in the C_{PM} is in the 2–5 μm range which is within the starting alumina particle size range [33], showing that the unreacted alumina particles are not involved in the chemical formation of the borate needle.

The whisker diameter as a function of the mean pore size distribution is plotted in Fig. 5. It is well known that in ceramic microstructures the mean pore size is generally correlated with the particle size distribution. This is definitively the case for the SP_{PM} materials, where the needle thickness is equivalent to the pore size distribution evaluated by mercury intrusion (Fig. 2). Apparently this is not correlated with the needle length, which is at least twenty times bigger than the diameter. On the other hand the C_{PM} borate and alumina grain sizes differ in one magnitude order, showing the effect of the presence of the unreacted alumina rounded particles of 2–5 μm.

From the performed microstructural – textural analysis (Sections 3.1 and 3.2) it can be held that the microstructural parameters are equivalent for the two antagonistic microstructural configurations (C_{PM} and S_{PM}).

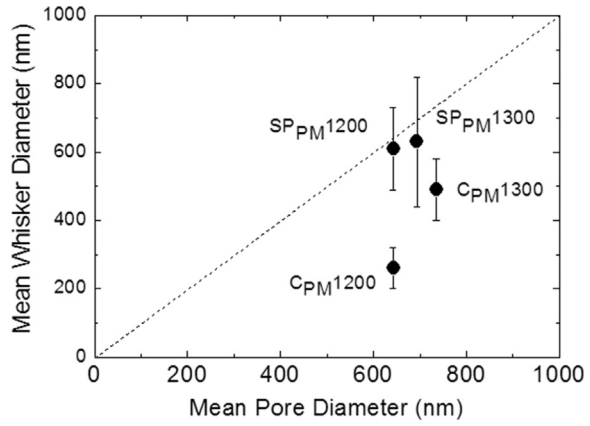

Fig. 5. Mean whisker diameter (WD) as a function of the mean pore diameter (PD); the WD = PD lines is plotted in dashes.

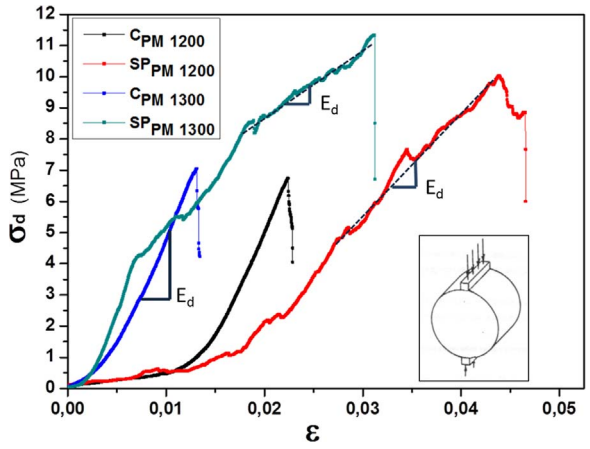

Fig. 6. Examples of the diametral stress strain curves of the SP_{PM} and the C_{PM} studied materials.

3.3. Diametral compression behavior

Typical stress–strain curves for C_{PM} and SP_{PM} materials are shown in Fig. 6. Values of mechanical strength and apparent Young modulus are shown in Table 4.

The initial region of stress–strain curves (see Fig. 6) showed a nonlinear segment that could be related to several factors: the arrangement of the specimen in the load system, the load distribution in the load contact region, and/or elastic strains of the load system [37,40]. This initial ε region was up to 0.0025 for materials fired at 1200 °C and up to 0.0125 for materials fired at 1300 °C.

For both the C_{PM} materials after this first region, an almost linear response was observed up to the sudden fall of the load due to the brittle behavior in which the specimen failed. Therefore, porous interlocking needle-rounded alumina grains composite microstructure presents a brittle behavior, like alumina ceramics [41–45]. The achieved strength was almost 7 MPa for both studied samples fired at 1200 and 1300 °C. The observed dispersion values were within the typical ones and slightly higher for the $C_{PM}1300$ material. From these measurements it can be stand that the mechanical strength of this C_{PM} is equivalent within the experimental error. This might be explained by the similar microstructure of these materials described above. The achieved values encourage the structural application of these composites.

On the other hand both SP_{PM} materials presented a different feature. These present a deviation from the linear brittle behavior. Particularly, these presented several discontinuities even at lower stresses. The tests were carried out at a relatively slow constant displacement rate; the effect of the rate was not studied. The measured discontinuities might be explained by the local collapse of the interlocked needles; which are micron size, described in Section 3.2. The global integrity of the disc samples was kept up to the final sudden collapse. After each discontinuity, a slight decrease in the strains stress slope was observed. This loss of stiffness confirmed the local deterioration. From this it can be concluded that the behavior would be definitively not reversible. No important effect of the firing temperature and whisker thickness was observed. The achieved values are similar or within the experimental error. However the maximum stress evaluated was higher in all the cases if compared with the other microstructural configuration. The achieved strength for the SP_{PM} materials was at least 30% higher than the C_{PM} materials, particularly 50% higher for materials fired at 1300 °C. The observed deviations were below 11% showing the goodness of this mechanical characterization. This fact coupled with the lower thermal conductivity (Table 2) would encourage the insulating applications of this particular type of material.

It is worth to point out that although the stress strain behavior was not strictly linear, the final slope was possibly calculated; the last

Table 4
Mechanical properties of the studied materials.

Sample	σ_d (MPa)	Standard deviations	Relative error (%)	E_d (MPa)	Standard deviations	Relative error (%)
$C_{PM}1200$	6.9	0.6	9.2	630	90	14.1
$C_{PM}1300$	6.4	1.2	18.0	590	70	12.2
$SP_{PM}1200$	8.8	0.9	10.6	870	330	38.6
$SP_{PM}1300$	9.9	0.9	9.2	980	340	33.2

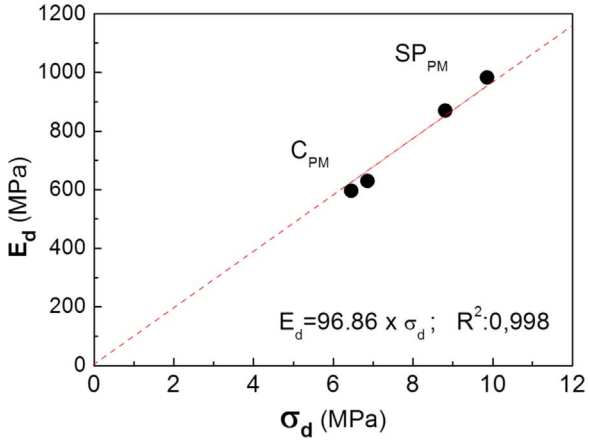

Fig. 7. Apparent elastic modulus (E_d) as a function of the diametral compression resistance (σ_d), and linear fitting.

section (25%) of the stress strain curve was employed for the slope estimation.

In general the evaluated stiffness (E_d) presents very low values in comparison with other ceramic materials; this distinctive result is explained by the present porosity, described above combined with the interlocked whisker microstructure. The evaluated E_d for both the C_{PM} materials is, as the strength, equivalent for the two evaluated materials. This is expected due to the equivalent phase composition and microstructure. The reported single crystal stiffness of the $Al_{18}B_4O_{33}$ crystal is 400 GPa [12], and alumina young modulus is ≈300 GPa. These are around 5.10^5 times the stiffness of the present complex interlocked needle porous microstructure. The calculated stiffness of the SP_{PM} is slightly higher than the alumina containing composite (C_{PM}) materials. However under short displacements it can be easily observed that the slope might be higher for the SP_{PM}. As already described this subsequent discontinuities are accompanied by decreases in the local stress strain slope. The observed dispersion values for E_d are also eloquent; while the slope dispersion is below 15% for the brittle C_{PM} it is almost 40% for the non-brittle SP_{PM} needle porous materials, showing the complexity of the behavior.

Finally there is a direct linear correlation between the two evaluated mechanical parameters E_d and σ_d. Fig. 7 shows the linear fitting plot between the evaluated parameters for both materials fired at two different temperatures. Roughly the stiffness value is one hundred times the diametral strength of this disc shape samples. The actual value of the performed linear fitting can be found within Fig. 7.

4. Conclusions

Two pairs of materials with respectively similar microstructures were processed by reaction sintering from boric acid and alumina. Two single ($Al_{18}B_4O_{33}$) phase porous whisker ceramics were compared with two Al_2O_3-$Al_{18}B_4O_{33}$ composite porous ceramic (1:1). The four showed comparable grain size and comparable apparent porosities, in diameter (≈0.7 μm) and in volume fraction (≈45%). Whisker thickness was in the 0.3 – 0.6 μm range. The aspect ratio was above 20 in all cases.

In general, the mechanical behaviors were well defined for both microstructural configurations. No important effect was observed for the firing temperature employed.

Single $Al_{18}B_4O_{33}$ phase porous materials presented high mechanical strengths, especially taking into account the developed porosities, reaching the 10 MPa for the $SP_{PM}1300$. This was 50% higher than the composite, which was below 7 MPa in both studied cases; which is also adequate. Taking into account that both materials presented low thermal conductivities the structural application is encouraged.

Within the respective microstructural configurations the whisker thickness did not affect significantly the mechanical behavior and parameters.

A well-defined fragile behavior was observed and described in the composite material. On the other side the single $Al_{18}B_4O_{33}$ needle porous material presented a distinctive behavior with local discontinuities with no loss of integrity in the diametral stress behavior and higher strength than the other configuration.

A very low apparent stiffness was clearly evaluated for the composite material (≈ 600 MPa). A more imprecise value was achieved for the single phase material, averaging 900 MPa. These values are remarkably lower than the constituent phases stiffness (around 300–500 GPa).

Finally, as a rule of a thumb the stiffness value is one hundred times the diametral strength of this disc shape samples of the present type of materials.

Acknowledgments

This work has been partially supported by Nano-Petro FONARSEC Project 2012 (ANPCyT). MFH acknowledges CONICET and Y-Tec for the fellowship.

References

[1] I. Nettleship, Applications of porous ceramics, Key Eng. Mater. 122–124 (1996) 305–324.
[2] A.R. Studart, et al., Processing routes to macroporous ceramics: a review, J. Am. Ceram. Soc. 89 (6) (2006) 1771–1789.
[3] T. Ohji, M. Fukushima, Macro-porous ceramics: processing and properties, Int. Mat. Rev. 57 (2012) 115–131.
[4] C. Baudin, Processing of alumina and corresponding composites, Compr. Hard Mater. 2 (2014) 31–72.
[5] S.P. Ray, Preparation and characterization of aluminum borate, J. Am. Ceram. Soc. 75 (1992) 2605–2609.
[6] K.P. Peil, L.G. Galya, G. Marcelin, Acid and catalytic properties of nonstoichiometric aluminum borates, J. Catal. 115 (1989) 441–451.
[7] S.A. El-Hakam, E.A. El-Sharkawy, Structural characterization and catalytic properties of aluminum borates–alumina catalysts, Mater. Lett. 36 (1998) 167–173.
[8] J. Wang, G. Ning, Y. Lin, Chemical synthesis of $Al_{18}B_4O_{33}$ whiskers via a combustion method, Mater. Lett. 62 (2008) 2447–2449.
[9] H. Zhao, Y. Krysiak, K. Hoffmann, B. Barton, L. Molina-Luna, R.B. Neder, U. Kolb, Elucidating structural order and disorder phenomena in mullite-type Al 4 B 2 O 9 by automated electron diffraction tomography, J. Solid State Chem. 249 (2017) 114–123.
[10] K. Hoffmann, T.J.N. Hooper, M.M. Murshed, O. Dolotko, Z. Révay, A. Senyshyn, R.X. Fischer, Formation, stability and crystal structure of mullite-type Al 6– x B x O 9, J. Solid State Chem. 243 (2016) 124–135.
[11] G. Lin, L. Guan, K.M. Lü, Effects of whisker surface treatment on microstructure and properties of Al18B4O33/6061Al composites, Trans. Nonferr. Met. Soc. 20 (2010) 349–354.
[12] K. Suganuma, T. Fujita, G. Sasaki, N. Suzuki, Evaluation of strength and heat-resistance for aluminum-borate whisker reinforced AC8A aluminum alloy composite, J. Jpn. Inst. Light Met. 41 (1991) 270–275. http://dx.doi.org/10.2464/jilm.41.270.

[13] M. Yoshida, S. Takeuchi, J. Pan, G. Sasaki, N. Fuyama, T. Fuj, H. Fukunaga, Preparation and characterization of aluminum borate whisker reinforced magnesium alloy composites by semi-solid process, Adv. Compos. Mater. 8 (1999) 259–268.
[14] Chun Cheng, X.X. Ding, F.J. Shi, Yun Cheng, X.T. Huang, S.R. Qi, C. Tang, Preparation of aluminum borate nanowires, J. Cryst. Growth 263 (2004) 600–604.
[15] L.M. Peng, X.K. Li, H. Li, J.H. Wang, M. Gong, Synthesis and microstructural characterization of aluminum borate whiskers, Ceram. Int. 32 (2006) 365–368.
[16] Y. Li, R.P.H. Chang, Synthesis and characterization of aluminum borate ($Al_{18}B_4O_{33}$, $Al_4B_2O_9$) nanowires and nanotubes, Mater. Chem. Phys. 97 (2006) 23–30.
[17] E.M. Elssfah, H.S. Song, C.C. Tang, J. Zhang, X.X. Ding, S.R. Qi, Synthesis of aluminum borate nanowires via a novel flux method, Mater. Chem. Phys. 101 (2007) 499–504.
[18] S. Peng, H. Jinwen, W. Wenwei, Preparation of aluminum borate whiskers by the molten salt synthesis method, Ceram. Int. 39 (2013) 7263–7267.
[19] R.K. Gupta, A.A. Al-Ghamdi, O.A. Al-Hartomy, F. Al-Hazmi, F. El-Tantawy, F. Yakuphanoglu, Synthesis and characterization of nanostructured aluminum borate by sol–gel method, J. Sol-Gel Sci. Technol. 64 (2012) 100–103.
[20] J. Zhou, D. Su, J. Luo, M. Zhong, Synthesis of aluminum borate nanorods by a low-heating-temperature solid-state precursor method, Mater. Res. Bull. 44 (2009) 224–226.
[21] I.E. Gonenli, A.C. Tas, Chemical preparation of aluminum borate whiskers, Powder Diffr. 15 (2000) 104–107.
[22] J. Wang, G. Ning, X. Yang, Z. Gan, H. Liu, Y. Lin, Large-scale synthesis of $Al_4B_2O_9$/$Al_{18}B_4O_{33}$ whiskers via a novel method, Mater. Lett. 62 (2008) 1208–1211.
[23] Y. Liu, Q. Li, S. Fan, Self-catalytic growth of aluminum borate nanowires, Chem. Phys. Lett. 375 (2003) 632–635.
[24] Z. Yu, N. Zhao, E. Liu, C. Shi, X. Du, J. Wang, Low-temperature synthesis of aluminum borate nanowhiskers on the surface of aluminum powder promoted by ball-milling pretreatment, Powder Technol. 212 (2011) 310–315.
[25] H.K. Lee, S. Zerbetto, P. Colombo, C.G. Pantano, Glass–ceramics and composites containing aluminum borate whiskers, Ceram. Int. 36 (2010) 1589–1596.
[26] X. Song, W. Liu, J. Wang, S. Xu, B. Liu, J. Liu, Y. Ma, Microstructural differences between electrospun alumina borate nanofibers prepared by solutions with different PVP contents (Available online)Ceram. Int. (2017) 28. http://dx.doi.org/10.1016/j.ceramint.2017.04.163.
[27] T.M. Souza, A.P. Luz, C. Pagliosa, V.C. Pandolfelli, Mineralizing alumina-magnesia cement-bonded castables containing magnesium borates, Ceram. Int. (2015). http://dx.doi.org/10.1016/j.ceramint.2015.05.063.
[28] A.P. Luz, T. Santos, V.C. Pandolfelli, J. Medeiros, High-alumina boron-containing refractory castables, Int. J. Appl. Ceram. Technol. (2014). http://dx.doi.org/10.1111/ijac.12310.
[29] A.P. Luz, T. Santos, J. Medeiros, V.C. Pandolfelli, Sintering additive role on the performance of advanced refractory castables, in: Proceedings of the Unified International Technical Conference on Refractories, UNITECR 2013, 2014, pp. 1099–1104.
[30] A.P. Luz, A.B. Silva Neto, T. Santos Jr, J. Medeiros, V.C. Pandolfelli, Mullite-based refractory castable engineering for the petrochemical industry, Ceram. Int. 39 (8) (2013) 9063–9070. http://dx.doi.org/10.1016/j.ceramint.2013.05.001.
[31] M.A.L. Braulio, G.G. Morbioli, V.C. Pandolfelli, Advanced boron-containing Al_2O_3-MgO refractory castables, J. Am. Ceram. Soc. 94 (10) (2013) 3467–3472. http://dx.doi.org/10.1111/j.1551-2916.2011.04608.x.
[32] I.D. Giovannelli Maizo, A.P. Luz, C. Pagliosa, V.C. Pandolfelli, Boron sources as sintering additives for alumina-based refractory castables, Ceram. Int. (2017). http://dx.doi.org/10.1016/j.ceramint.2017.05.047.
[33] M.F. Hernández, G. Suárez, M. Cipollone, M.S. Conconi, E.F. Aglietti, N.M. Rendtorff, Formation, microstructure and properties of aluminum borate ceramics obtained from alumina and boric acid, Ceram. Int. 43 (2017) 2188–2195. http://dx.doi.org/10.1016/j.ceramint.2016.11.002.
[34] C. Volzone, N. Zagorodny, Mercury intrusion porosimetry (MIP) study of archaeological pottery from Hualfin Valley, Catamarca, Argentina, Appl. Clay Sci. 91–92 (2014) 12–15. http://dx.doi.org/10.1016/j.clay.2014.02.002.
[35] M.K. Fahad, J. Mater. Sci. 31 (1996) 3723. http://dx.doi.org/10.1007/BF00352786.
[36] C. Rocco, G.V. Guinea, J. Planas, M. Elices, Review of the splitting-test standards from a fracture mechanics point of view, cement, Concrete Res. 31 (2001) 73–82.
[37] M.L. Sandoval, M.A. Pucheu, M.H. Talou, A.T. Martinez, M.A. Camerucci, Mechanical evaluation of cordierite precursor green bodies obtained by starch thermogelling, J. Eur. Ceram. Soc. 29 (16) (2009) 3307–3317.
[38] M.F. Serra, M.F. Acebedo, M.S. Conconi, G. Suarez, E.F. Aglietti, N.M. Rendtorff, Thermal evolution of the mechanical properties of calcareous earthenware, Ceram. Int. 40 (1) (2014) 1709–1716.
[39] B.W. Darvell, J. Mater. Sci. 25 (1990) 757.
[40] M.L. Sandoval, M.H. Talou, A.T. Martinez, M.A. Camerucci, Mechanical testing of cordierite porous ceramics using high temperature diametral compression, J. Mater. Sci. 45 (18) (2010) 5109–5117.
[41] D. Hardy, D.J. Green, Mechanical properties of a partially sintered alumina, J. Am. Ceram. Soc. 15 (8) (1995) 769–775.
[42] S.C. Nanjangud, R. Brezny, D.J. Green, Strength and Young's modulus behavior of a partially sintered porous alumina, J. Am. Ceram. Soc. 78 (1) (1995) 266–268.
[43] C.H. Schilling, et al., Ultrasonic and mechanical behavior of green and partially sintered alumina: effects of slurry consolidation chemistry, J. Am. Ceram. Soc. 81 (10) (1998) 2629–2639.
[44] S.J. Glass, D.J. Green, Permeability and infiltration of partially sintered ceramics, J. Am. Ceram. Soc. 82 (10) (1999) 2745–2752.
[45] M. Guazzato, et al., Strength, fracture toughness and microstructure of a selection of all-ceramic materials. Part I. Pressable and alumina glass-infiltrated ceramics, Dent. Mater. 20 (5) (2004) 441–448.